Letters in Applied NanoBioScience
Open-Access Journal (ISSN: 2284-6808)

Article
Volume 13, Issue 1, 2024, 1
https://doi.org/10.33263/LIANBS131.001

Evaluation of $MnWO_4$ Nanomaterial for Enhanced Photocatalytic Degradation Activity Over Methyl Orange Dye

Princy Jayakumar [1], Suganya Palani [1], Mathivanan Nallathambi [1], Krishnasamy Kuppusamy [1,*]

[1] Department of chemistry, Annamalai university, Annamalai Nagar, Chidambaram, Tamil Nadu, India, Pin code-608002
* Correspondence: krishnasamybala56@g-mail.com (K.K.);

Scopus Author ID 17346420400

Received: 28.09.2022; Accepted: 12.10.2022; Published: 25.02.2023

Abstract: Among several metal oxide nanoparticles, WO_3-$MnWO_4$ play a vital role in various nanoscience applications, including photocatalytic activity, due to their physicochemical properties. In this study, WO_3-$MnWO_4$ nanomaterials were synthesized by the facile hydrothermal method, and then the heterogeneous nanomaterials were characterized by various physicochemical methods viz.TG/DTA, UV-DRS, XRD, FT-IR, SEM, TEM-EDX, and XPS. After thorough characterization, an evaluation study was performed for photocatalytic degradation activity against Methyl Orange dye using sunlight irradiation. During this experiment, the reactants were simultaneously tested with different pH mediums, and the reaction was monitored constantly at regular intervals. A kinetics study was conducted, and the reaction was evaluated under UV-VIS spectroscopy to enumerate the degradation activity. In this experiment, both WO_3 and $MnWO_4$ demonstrated their efficiency for photocatalytic degradation activity against MO dye. The degradation activity was maximal in a neutral pH medium than in alkaline and acidic mediums. Further, when comparing these two nanomaterials, heterogeneous $MnWO_4$ exhibited higher degradation efficiency than homogenous WO_3. Here, we confirmed that the monoclinic nanostructured WO_3-$MnWO_4$ has the potential to have a profound impact on the dye degradation process and, thereby, the efficient removal of hazardous environmental pollution.

Keywords: $MnWO_4$ nanomaterial; photocatalytic activity; methyl orange; effect of pH.

© 2023 by the authors. This article is an open-access article distributed under the terms and conditions of the Creative Commons Attribution (CC BY) license (https://creativecommons.org/licenses/by/4.0/).

1. Introduction

Over the past decades, the photocatalytic degradation process has been considered advantageous for removing organic contaminants because of its effectiveness, minimal chemical waste, ease of labor, and affordability. Removing environmental pollutants and sewage contaminants are major problems encountered worldwide [1]. Several methods are available to improve the efficiency of currently available photocatalysts, such as doping, band-gap tailoring, morphology alteration, and modifying the crystal lattice to resolve [2]. Photocatalysts that are involved in the removal of organic pollutants also could be involved in several other applications like water treatment, hydrogen evolution reaction, oxygen evolution reaction, Nitrogen oxides(NOx)Oxidation, CO_2 reduction in fuels, and as disinfectants [3-5]. So far, semiconducting materials such as metal oxides, sulfides, and phosphides have attracted the enormous recognition of researchers because of their surface structures and wide band-gap area. Among several metal oxide nanoparticles, ZnO, TiO_2, SnO_2, CuO, and WO_3 have been

enormously used as photocatalysts. WO_3 distinctively plays a crucial role in environmental pollution remediations. WO_3 is an n-type semiconductor metal oxide with a high tunable configuration, better conductivity, non-toxic, and cost-effective [6,7]. WO_3 offers a wide-band gap area of nearly 2.5 to 2.7 eV and a larger surface area to enhance the catalytic process. Moreover, oxygen vacancies are present to maintain the stable crystal structure of nanomaterial by reducing the band bending and sustaining the structural integrity of the WO_3 nanomaterial [8,9]. In photocatalytic activity, WO_3 can produce photogenerated carriers to form electron-hole pairs to degrade the organic contaminants. Further, this study focused on evaluating the photocatalytic activity of WO_3 along with $MnWO_4$ as $MnWO_4$ nanostructures exhibit one of the dominant tungstate characteristics, the efficient photocatalytic activity, and also have potential electrochemical and biological activities [10,11]. Though there are several methods employed in the fabrication of nanomaterials, such as Hydrothermal [12,13], Co-precipitation [14,15], Sol-gel [16], Combustion [17], Ball milling [18,19], Microemulsion [20] and Sono synthesis [21], the hydrothermal approach gives better crystalline nature, eco-friendliness and also provides minimum loss of material. Hence, an attempt was made to synthesize the WO_3 and $MnWO_4$ nanoparticles via the cost-effective hydrothermal approach, and its photocatalytic activity has been studied and discussed suitably.

2. Materials and Methods

2.1. Materials.

All the chemicals used in this experiment are analytical quality reagents, and they are used without any further purification. Sodium tungstate dihydrate, Hydrochloric acid, Cetyltrimethylammonium bromide, and Manganese chloride tetrahydrate are the chemicals used in this experimental method.

2.2. Synthesis of Tungsten oxide.

Initially, 2gms of sodium tungstate dihydrate ($Na_2WO_4.2H_2O$) was dissolved in 40 ml of deionized water. Hydrochloric acid was added to maintain pH, followed by the addition of cetyltrimethylammonium bromide solution (CTAB) and stirred continuously for 30 minutes at room temperature. The prepared solution was transferred into a Teflon-lined autoclave and maintained at 150°C for 12 hours. The resultant precipitate was washed with distilled water and ethanol. Finally, the dried product was annealed at 400°C for 3 hours (Scheme 1).

2.3. Synthesis of Manganese tungstate.

Similar to Tungsten oxide synthesis, 2gms of Sodium tungstate dihydrate was mixed in 40 ml of deionized water, and hydrochloric acid was added to maintain pH, then cetyltrimethylammonium bromide solution (CTAB) was added, and the mixture was constantly agitated for 30 minutes at room temperature. In addition, the precursor manganese chloride tetrahydrate (MnCl2.4H2O) was dissolved using deionized water and added slowly to the above mixture. The entire solution was stirred thoroughly. The mixture was transferred into the Teflon-lined stainless steel autoclave and maintained up to 180°C for 16 hours. The obtained precipitate was collected and sequentially washed with distilled water. The procured product was calcinated at 450°C for 2 hours (Scheme 1).

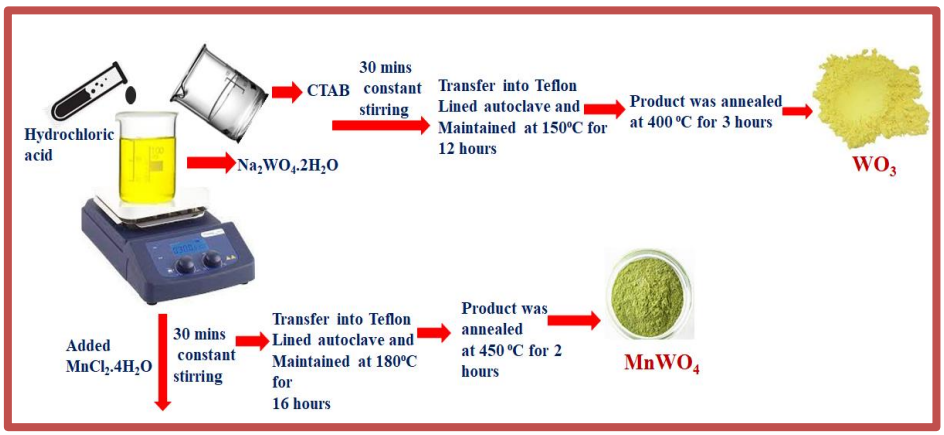

Scheme 1. Preparation of the synthesized WO_3 and $MnWO_4$ nanomaterials.

3. Results and Discussion

3.1. TG/DTA analysis.

The thermal stability of WO_3 and $MnWO_4$ nanomaterials was investigated using TG/DTA analysis. In (Figure.1 WO_3 and $MnWO_4$), the TG/DTA curve shows the two steps of the thermal degradation process in WO_3. The first step of weight loss occurred at 300° C due to the removal of water molecules, and the weight percentage loss was 25%. The second step of weight loss occurred between 400°C to 700°C, and the weight loss percentage was 5%. $MnWO_4$ nanomaterial follows a similar process of weight loss to WO_3. The initial weight loss at 200° C by 6%, and the second step degradation between 300 to 400°C resulted in a weight loss of 7%. The third step of weight loss is between 400 to 800°C with a weight loss percentage of 4% [22]. Furthermore, the endothermic and exothermic peaks were observed at TG and DTA curves. TG exhibited endothermic peaks because of molecular relaxation. DTA peaks showed an exothermic process. However, WO_3 exothermic peaks were observed at nearly 200°C, whereas $MnWO_4$ exothermic peaks were observed at 600°C. Based on the TG/DTA analysis, the samples were fixed at the calcinated temperature of 450°C [23].

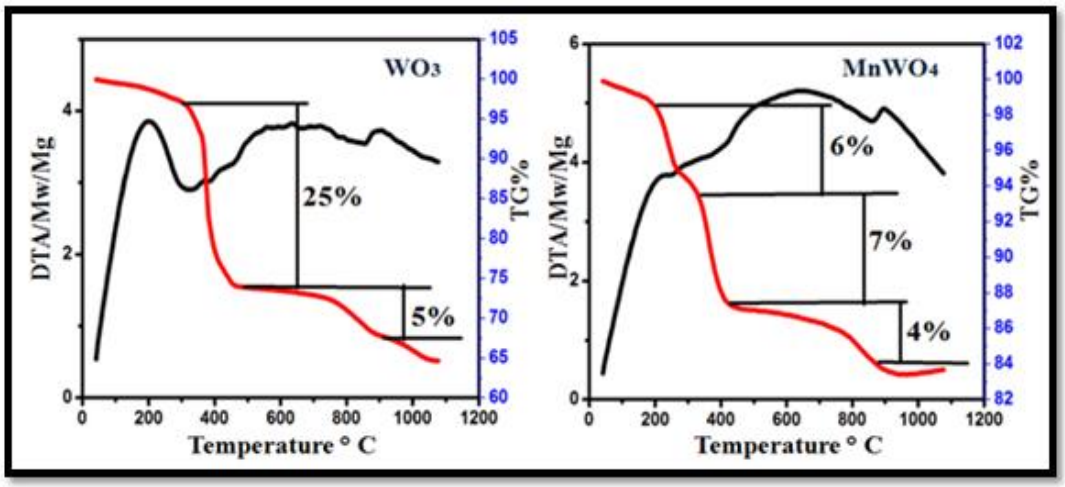

Figure 1. TG-DTA Curves of synthesized WO_3 and $MnWO_4$ nanomaterials.

3.2. XRD analysis.

The crystalline size and phase purity of the prepared nanomaterials were analyzed by XRD (Figure.2 WO_3 and $MnWO_4$). The diffraction peaks of WO_3 were observed at 2θ degrees

24.46, 26.54, 34.16, 35.55, 49.9, 53.57, 54.26, 59.98, 76.61 and are well-matched with JCPDS Card No 83-0950 corresponding to the plane (200), (120), (202), (122), (400), (331), (204), (224) and (116**)** which confirms the formation of monoclinic tungsten oxide.

Simultaneously, manganese tungstate nanoparticles appeared at 2θ degrees 23.65,24.25,34.04,44.27,47,20.48.18 and 62.20 and were well-matched to JCPDS Card No130434 and the corresponding planes are (011), (110), (002) (211), (030), (220) and (311) respectively. The crystalline size was enumerated by the Debye-Scherer equation (1) [24,25].

$$\text{Eq.No (1) : } D = 0.9n\lambda/\beta\cos\theta$$

λ is the x-ray wavelength, β is the line broadening at half the maximum intensity (FWHM), θ is Braggs angle, and 0.9 is the constant value for the crystalline shape. This equation obtained the crystalline size of WO3 and MnWO4 as 32 nm and 28 nm, respectively. No other peaks were observed during analysis, confirming the nanomaterial's purity.

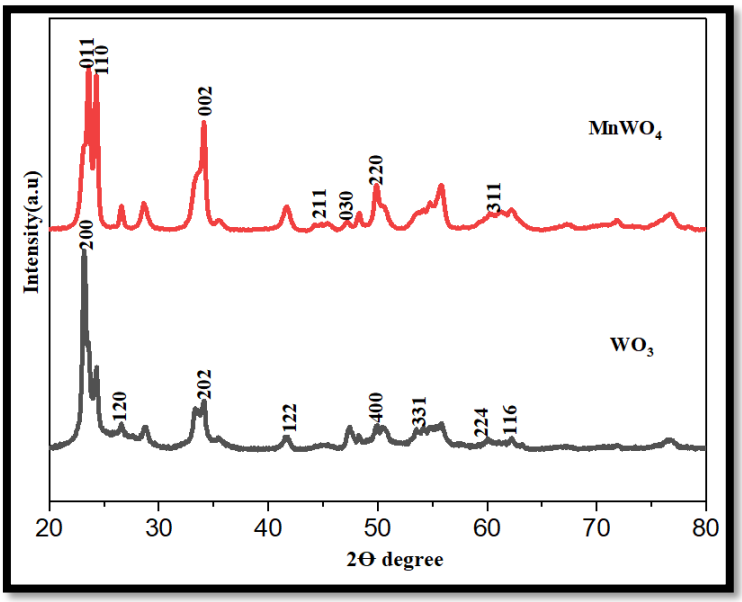

Figure 2. XRD Pattern of the Synthesized WO_3 and $MnWO_4$ nanomaterials.

3.2.1. Relation between Crystalline size and photocatalytic activity.

Crystalline size and crystallinity are significant factors affecting photocatalytic activity. The material's crystallinity had a significant impact on photocatalytic capabilities. A smaller crystallite produces greater surface areas, improving reactant adsorption and enhancing photo-reactivity. The photodegradation rate of the organic substrate will accelerate if the photocatalyst's surface area is increased because the number of active sites increases with increasing the surface area. This is because materials with high surface areas have more active sites than those with low surface areas. The monoclinic phase of the WO_3 was chosen as it has the most active catalytic performance and the most stable crystalline structure. In this study, heterogenous $MnWO_4$ had a smaller crystalline size and larger surface area compared with WO_3 homogenous material. Hence, surface area is the most important component in the photodegradation of organic substrates. [26,27].

3.3. Structural and morphological analysis.

The surface morphology of the synthesized nanomaterial was analyzed by SEM and TEM micrographs. The SEM micrographs in (Figure.3) show the different magnifications of

synthesized nanomaterials. The WO_3 image appeared with a quasi-spherical structure. The image of $MnWO_4$ shows uniformly agglomerated $MnWO_4$ nanoparticles on the smooth surface edges of WO_3. Whereas the TEM images manifest that all $MnWO_4$ nanoparticles have finite morphology, densely interconnected and spherical. The same was observed in the inert histograms during the study [24,25]. In (Figure 4) TEM-EDX analysis, WO_3 that appeared as irregular quasi manifested the spherical shape, and it were also observed that $MnWO_4$ nanostructures were agglomerated on the tungsten oxide surface. The selected area electron diffraction pattern (SAED pattern) confirms the crystalline nature of nanomaterials by showing the structural resemblance exhibited in (Figure 5).

Further, the SAED patterns were also compared with XRD patterns, which were highly correlated. Thus, the crystalline structure of the nanomaterials was characterized and validated. The EDX analysis technique was used to identify the elemental composition of nanostructures [28-30]. Mn, W, and O are the elements that were present in the catalyst. Mn, W, and O have weight percentages of 0.11, 57.06, and 13.97, respectively, and carbon is also dispersed in these nanostructures, which EDX confirmed. The monitoring described above demonstrated that the tungsten oxide was tightly bound to the metal and had developed into nanomaterial formations.

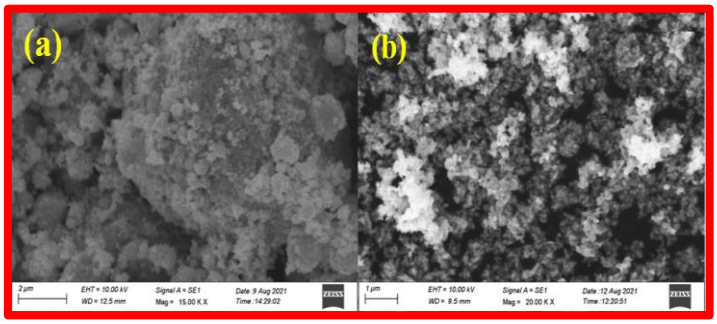

Figure 3. SEM images of Synthesized (a)WO_3 and (b) $MnWO_4$ nanomaterial.

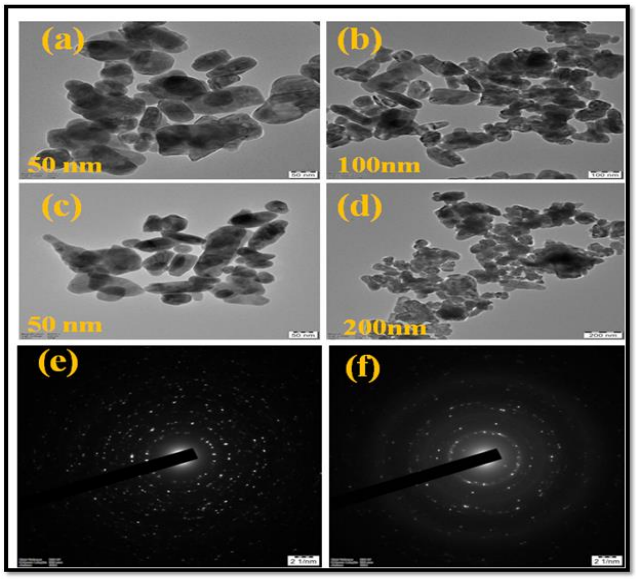

Figure 4. TEM micrographs of (a),(b) WO_3 and (c),(d) $MnWO_4$ nanomaterials and SAED pattern of prepared nanomaterials (e) WO_3 and (f) $MnWO_4$.

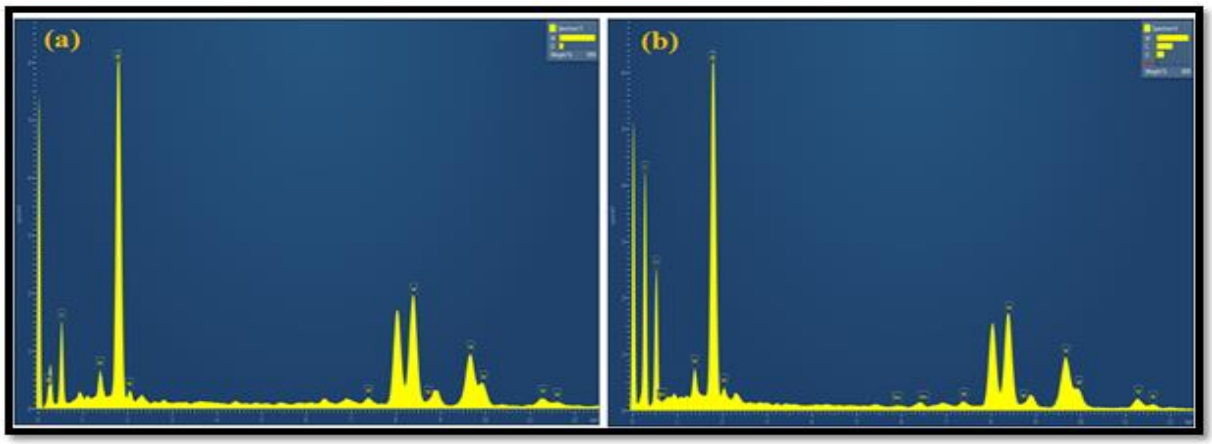

Figure 5. EDX spectrum of (a) WO_3 and (b) $MnWO_4$ nanomaterial.

3.4. FT-IR analysis.

The functional group analysis was employed to confirm the presence of various stretching and bending vibrations. The peaks were observed between 4000 cm^{-1} to 500 cm^{-1} wavenumbers in (Figure 6) The peak at 816 cm^{-1} is attributed to the WO_3 and shows the stretching vibration of bridging oxygen atoms between the O-W-O. It confirmed the presence of peroxo groups. The peak obtained at 1628 cm^{-1} represents the C=O group, and the 2924 cm^{-1} peak revealed the C=H group. The large peak stabilizes the tungsten oxide structure at 3433 cm-1, which reveals the H2O and indicates the presence of H-O-H hydroxyl molecules. A major peak centered at 741 and 813cm^{-1} is due to Mn-O stretching vibration groups [31].

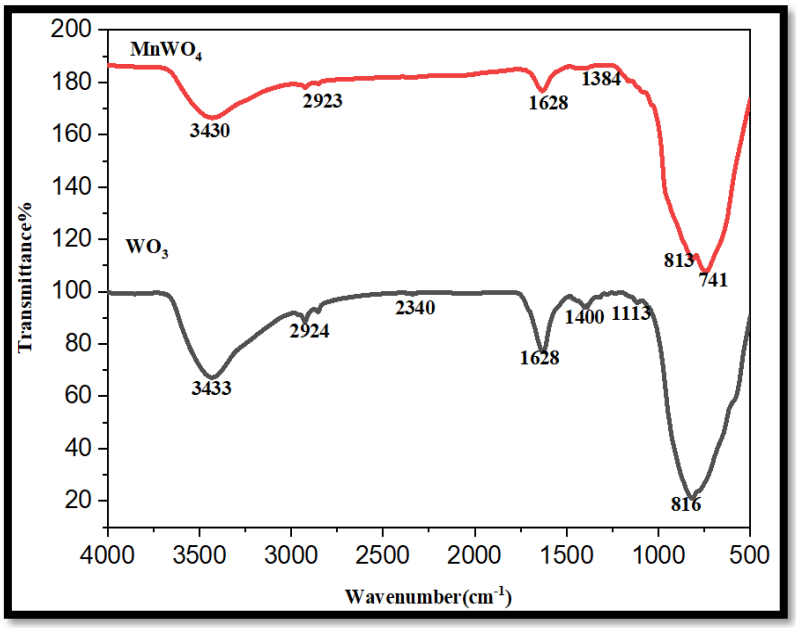

Figure 6. FT-IR analysis of synthesized WO_3 and $MnWO_4$ nanomaterials.

3.5. XPS analysis.

The chemical composition and exact ionic state of the elements in $MnWO_4$ were confirmed by X-ray photoelectron spectroscopy. In this study, the high-resolution peaks confirmed the presence of Mn, W, O, and N and, thereby, the expected composition of the synthesized $MnWO_4$ nanomaterial (Figure 7). The high-resolution peaks were measured by their intensity against the binding energy eV. The exact ionic states of the Mn2p deconvoluted

peaks were obtained at 643eV and 653eV. Thus, Mn $2p_{3/2}$ and Mn $2p_{1/2}$ orbital states affirmed the oxidation states of Mn^{2+}, respectively. The survey spectrum of W 4f was represented by two high-resolution peaks at 35.6eV and 38eV. The core O1s peak was obtained at 530eV. The high-resolution peak from the C1s spectrum describes the bond between carbon and hydrogen atoms to produce the CH and CC = bonds in $MnWO_4$ [32,33]. Furthermore, the high-resolution peaks around each component amply demonstrated the composition's integrity. The peaks obtained at the higher binding energies demonstrate the strong interaction between the WO_3 and Mn of $MnWO_4$, executing the compound as a superior nanomaterial.

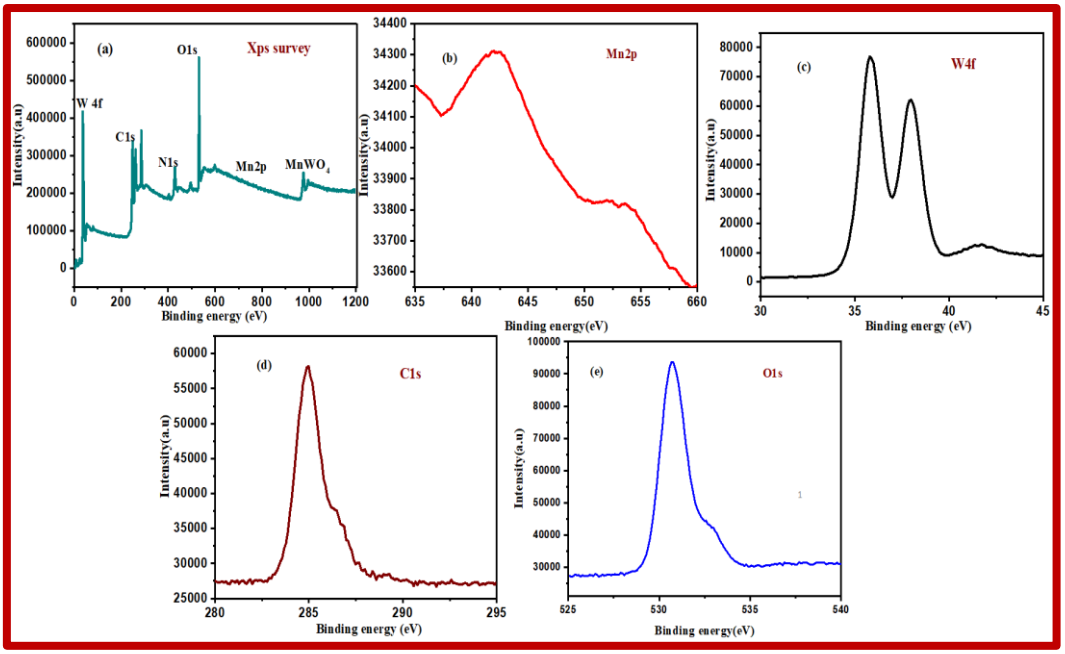

Figure 7. XPS survey scan of $MnWO_4$ nanomaterial and High-resolution XPS spectrum of $MnWO_4$ (a) XPS survey plot (b) Mn 2p (c) W 4f (d) C 1s (e) O 1s.

3.6. UV-DRS analysis.

UV-DRS spectra of the synthesized WO_3 and $MnWO_4$ are shown in (figure. 8). The prepared nanomaterials manifested high-optical quality in the UV region at the wavelength range of 300 to 800 nm. The spectrum of $MnWO_4$ had slightly shifted due to adding the host matrix, manganese ions [34]. Since WO_3 has a larger energy gap than $MnWO_4$ due to direct transitions between the nanomaterials, the crystalline size of WO_3 is higher than $MnWO_4$. Band-gap energy values were estimated using tauc plots.

Eq.No (2): $(\alpha.h\upsilon)1/y=B(h\upsilon-Eg)$

Where α is the absorption coefficient, h is the Planck constant,υ is the photon's frequency, E_g is the band-gap energy, and B is the constant. Y is the factor that depends on the nature of electron transition and is equal to ½ or 2 for the direct and indirect transition band gaps, respectively. The calculated Band gap values of WO_3 are 2.5 eV & $MnWO_4$ is 2.7eV [35]. These values matched well with reflectance spectra, confirm the $MnWO_4$ nanomaterial would exhibit an efficient photo response in the visible region than WO_3 due to its wide band gap.

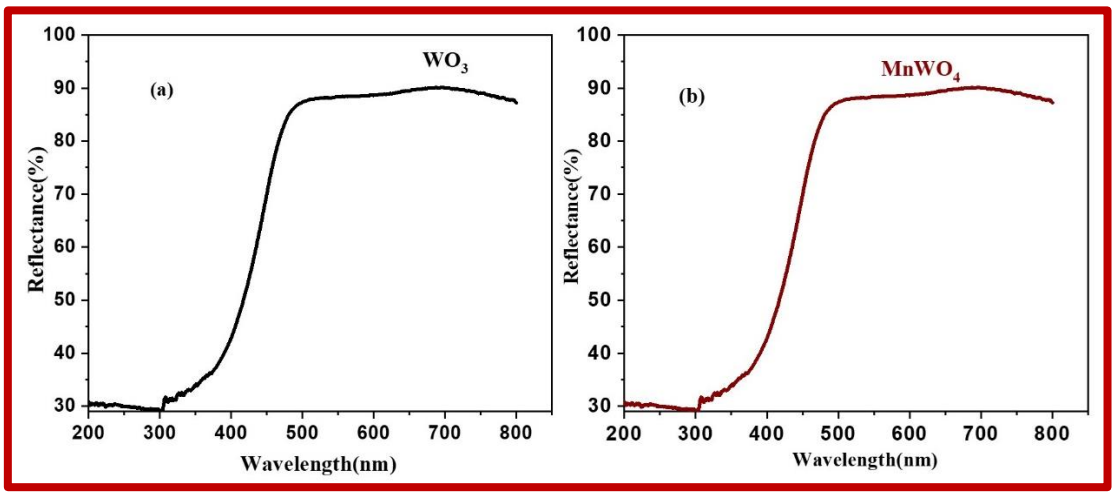

Figure 8. UV-DRS Spectrum of Synthesized (a)WO_3 and (b)$MnWO_4$ nanomaterials.

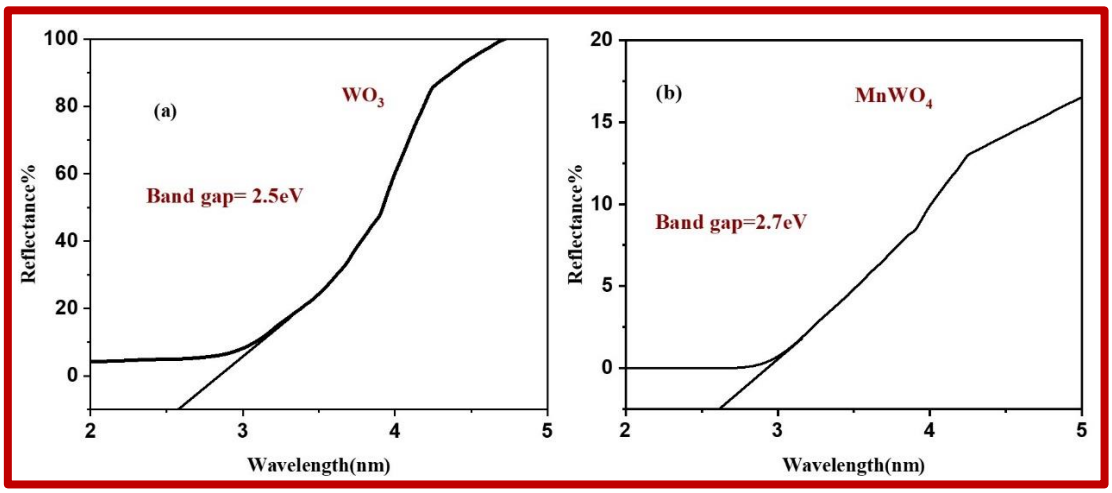

Figure 9. Tauc's plot of Synthesized (a) WO_3 and (b) $MnWO_4$ nanomaterials.

3.6.1. Relation between Electronic band structure and photocatalytic activity.

UV-visible spectroscopy can be used to calculate the band gap. A photocatalyst's electronic band structure and band-gap energy remarkably impact its photocatalytic performance. The band-gap energy is required to expand light absorption into the visible area and effectively use solar energy. An efficient photocatalyst needs band-gap energy between 2 eV - 3 eV. The energy band gap of tungsten oxide ranges between 2.7 and 2.8 eV, appeared in (Figure 9) WO_3 is a potential photocatalyst as it demonstrates strong photoabsorption in visible light. This means that WO_3 can be activated inside using a domestic light source and outside using sunlight. $MnWO_4$ is also a very efficient material due to its ideal band gap of 2.7 eV, which can efficiently absorb visible light, relatively high stability, outstanding reactivity, and other properties.[35,36] In this paper, the calculated band gap energy values of WO_3 and $MnWO_4$ were 2.5 and 2.7eV. Hence, these nanomaterials are strongly suggested to be superior photocatalysts.

3.7. Evaluation of photocatalytic performance.

The successfully prepared and characterized WO_3 and $MnWO_4$ nanomaterials have been experimented with for their photocatalytic activity in removing potent environmental pollutants. This study used methyl orange dye, and the experiment was conducted under sunlight irradiation with different pH mediums. Before exposing the dye to the nanomaterials,

it was optimized using UV-vis spectroscopy [37]. The optimal concentration for the experiment was obtained based on the UV study. The optimal concentration of methyl orange dye is 1×10^{5} M in an aqueous solution. The strong peaks of the dye were observed between 300nm to 600nm Figure.10. The reaction was observed with regular time intervals of every 10 minutes from the 15^{th} minute of total 65 minutes of study [38]. The photocatalytic degradation activity was enumerated for both the nanomaterials for the given conditions.

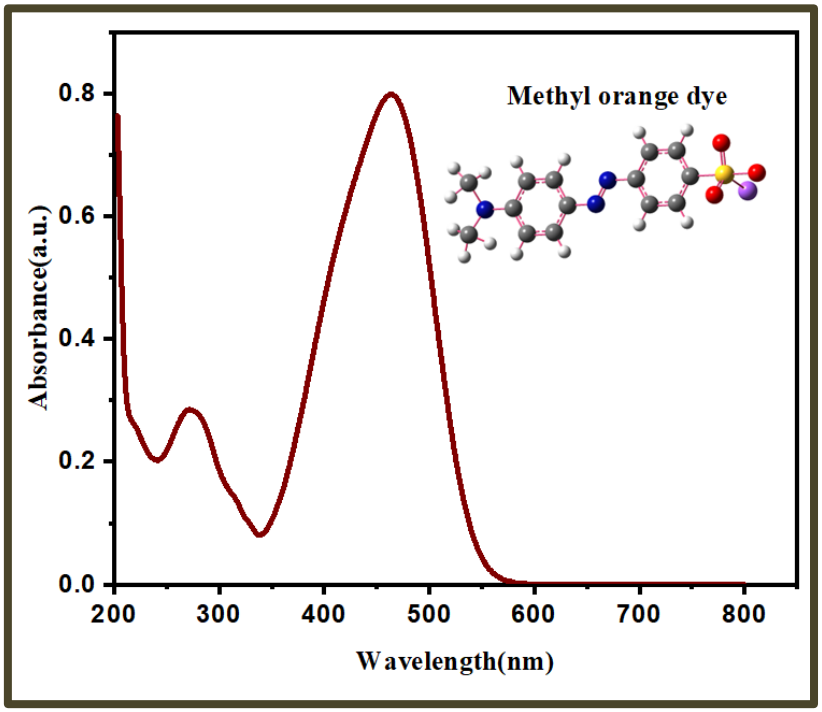

Figure 10. The UV-Visible spectrum of Optimized methyl orange dye.

3.7.1. Kinetic studies.

The Methyl orange dye was taken in different pH mediums, added with WO_3 and $MnWO_4$ individually, and exposed under sunlight irradiation. The reaction was monitored for the activity of nanomaterials upon Methyl orange dye. The experiment was observed and measured at regular time intervals. The degradation activity was analyzed under UV-Vis spectroscopy. The values were plotted in a graph by the degradation activity (reaction rate) against the irradiation time [39]. According to the kinetic studies, the constant rate values of this first-order reaction were calculated using the equation below.

Eq.No (3): $\ln (C_0/C_t) = -kt$

The observed rate constant values (k) in a Neutral medium are 0.01816 (s^{-1}), Alkaline medium, k=0.00544(s^{-1}), and In an acidic medium k=0.004606(s^{-1}), respectively.

3.7.2. Effect of pH.

pH plays a vital role in photocatalytic degradation. The effect of pH on the photodegradation of MO dyes was examined. The impact of pH in the experiment has been illustrated in (Figure. 11-16). The pH of the neutral medium was 7.0, the alkaline medium was between 9-12, and the acidic medium was between 2-4. The reaction was enumerated. It was measured that the degradation efficiency in the neutral medium for WO3 was 50% and for MnWO4 was 61%, in alkaline medium WO_3, given the degradation efficiency against the MO dye at 43% and $MnWO_4$ at 56%. In an acidic medium, it was 34% for WO_3 and 40% for

$MnWO_4$. According to the results, the maximum degradation efficiency was attained in the neutral medium (pH = 7). The neutral medium showed maximal degradation because of the strong binding of their H^+ cations and OH^- anions with a catalyst which would produce electron holes and super radicals. It leads to an enhanced oxidation process to degrade the colored wastewater(dye) compared to alkaline and acidic mediums [40,41].

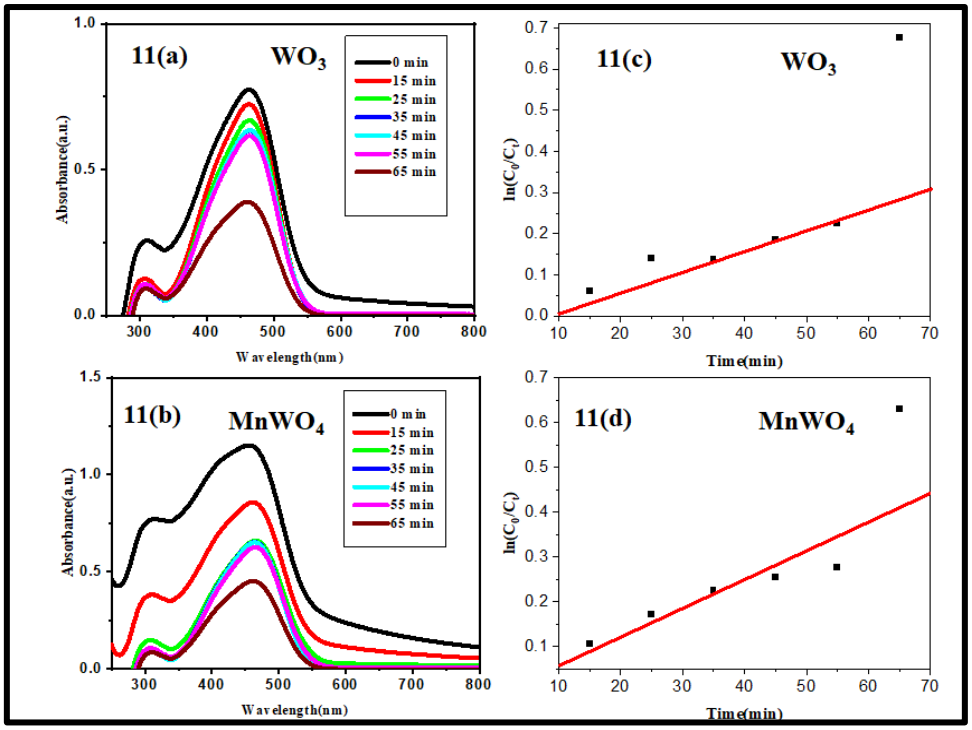

Figure 11. UV-Visible absorption spectra of the photocatalytic degradation of Methyl orange dye in the synthesized nanomaterials (a)WO_3,(b)$MnWO_4$, and plot of $ln(C_0/C_t)$ versus time(min) for the photocatalytic degradation of Methyl orange dye in the synthesized nanomaterials (c)WO_3 and (d)$MnWO_4$ in neutral medium (pH=7.0).

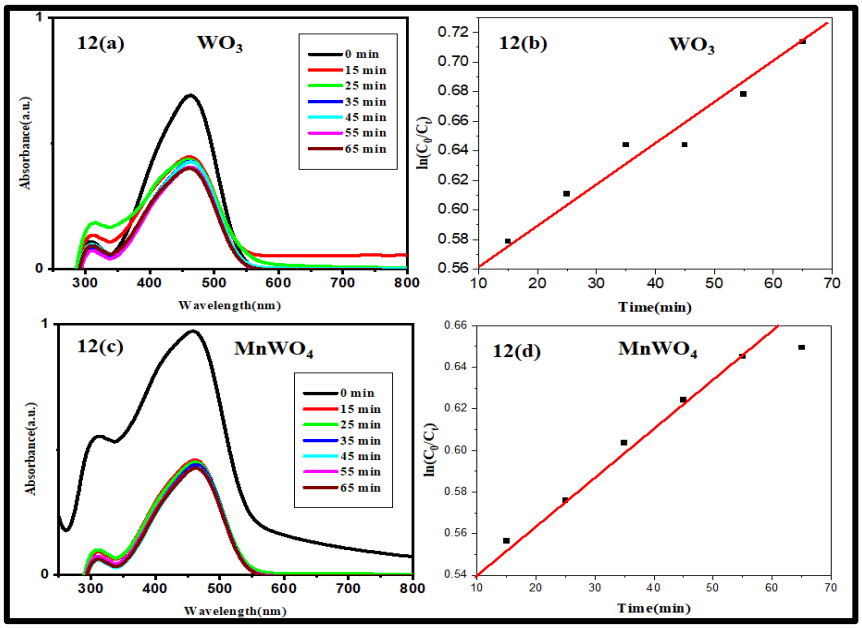

Figure 12. UV-Visible absorption spectra of the photocatalytic degradation of Methyl orange dye in the synthesized nanomaterials (a)WO_3,(b)$MnWO_4$, and plot of $ln(C_0/C_t)$ versus time(min) for the photocatalytic degradation of Methyl orange dye in the synthesized nanomaterials (c)WO_3 and (d)$MnWO_4$ in Alkaline medium (pH=9-12).

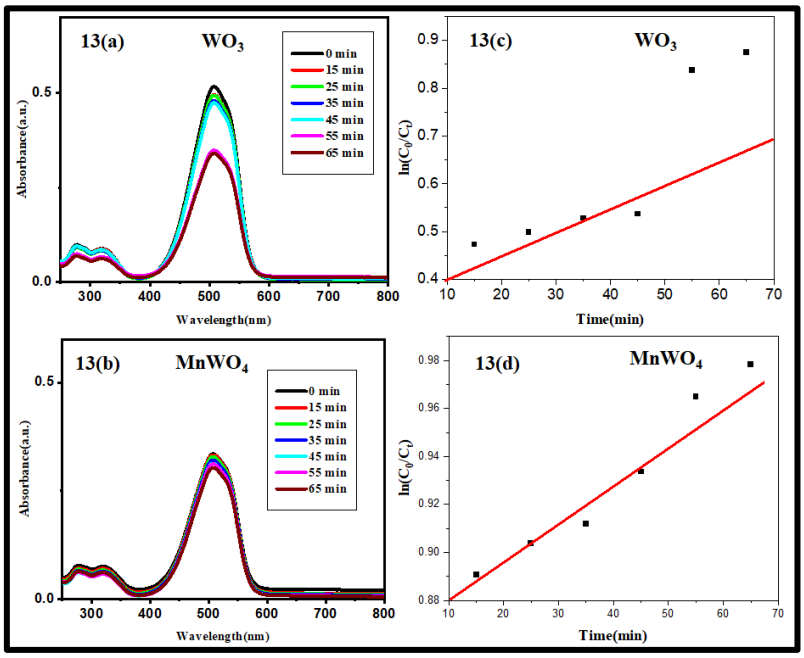

Figure 13. UV-Visible absorption spectra of the photocatalytic degradation of Methyl orange dye in the synthesized nanomaterials (a) WO_3,(b) $MnWO_4$, and plot of $ln(C_0/C_t)$ versus time(min) for the photocatalytic degradation of Methyl orange dye in the synthesized nanomaterials (c)WO_3 and (d)$MnWO_4$ in Acidic medium (pH=2-4).

3.7.3. Degradation efficiency of prepared nanomaterial.

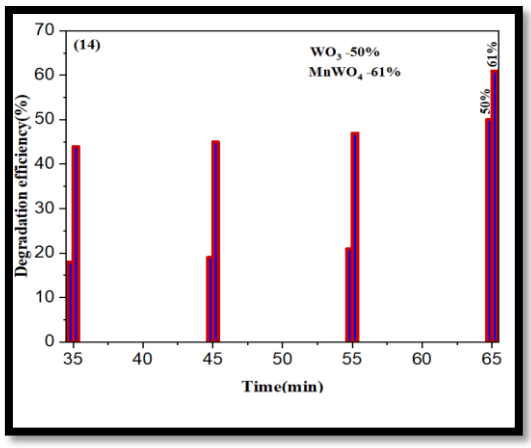

Figure 14. The plot of degradation efficiency versus time(min) for the prepared nanomaterials. Shows neutral medium pH=7.0.

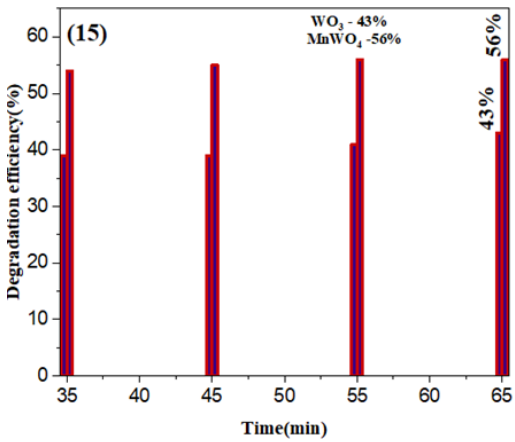

Figure 15. The plot of degradation efficiency versus time(min) for the prepared nanomaterials. Shows alkaline medium pH=9-12.

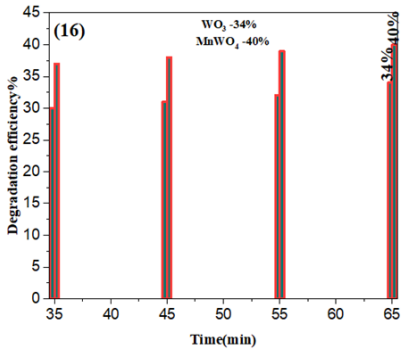

Figure 16. The plot of degradation efficiency versus time(min) for the prepared nanomaterials. Shows acidic medium pH=2-4.

3.7.4. Photocatalytic mechanism of prepared nanomaterials.

Figures 17 and 18 show schematic representations of the photocatalytic degradation process of MO dye by the WO_3 and $MnWO_4$ nanocomposites and graphical abstract of the photocatalytic degradation process of MO dye by the WO_3 and $MnWO_4$ nanocomposites. The photocatalytic mechanism of both WO_3 and $MnWO_4$ are similar. Under sunlight irradiation, the electron-hole pairs of e^- and h^+ are formed. The photogenerated electrons react with an oxygen (O_2) molecule to produce superoxide radicals. The photogenerated holes react with hydroxyl groups to form hydroxyl ions.

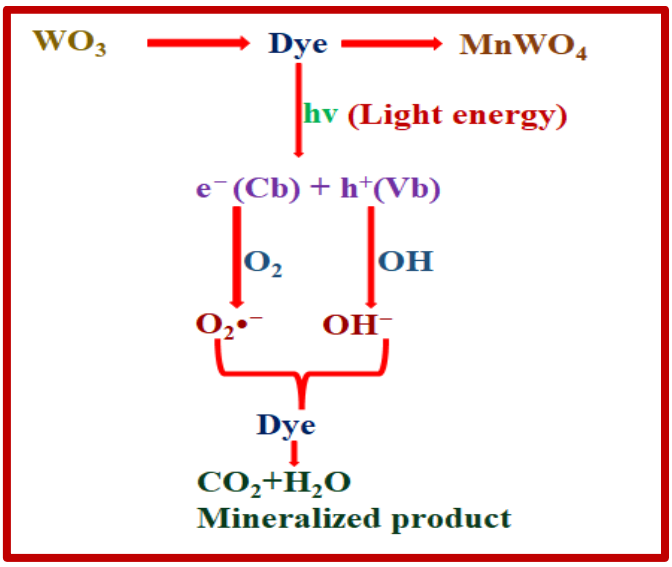

Figure 17. Schematic representation of the photocatalytic degradation process of MO dye by the WO_3 and $MnWO_4$ nanocomposites.

Further, the holes lead to the dissociation of water molecules [42]. The overall photocatalytic degradation mechanism of WO_3 and $MnWO_4$ is to create the energy band gaps and form the large surface area and thereby producing the super radicals and hydroxyl radicals. These hydroxyl radicals and superoxide radicals act upon the MO dye and break the macromolecules of organic pollutants [43-44].

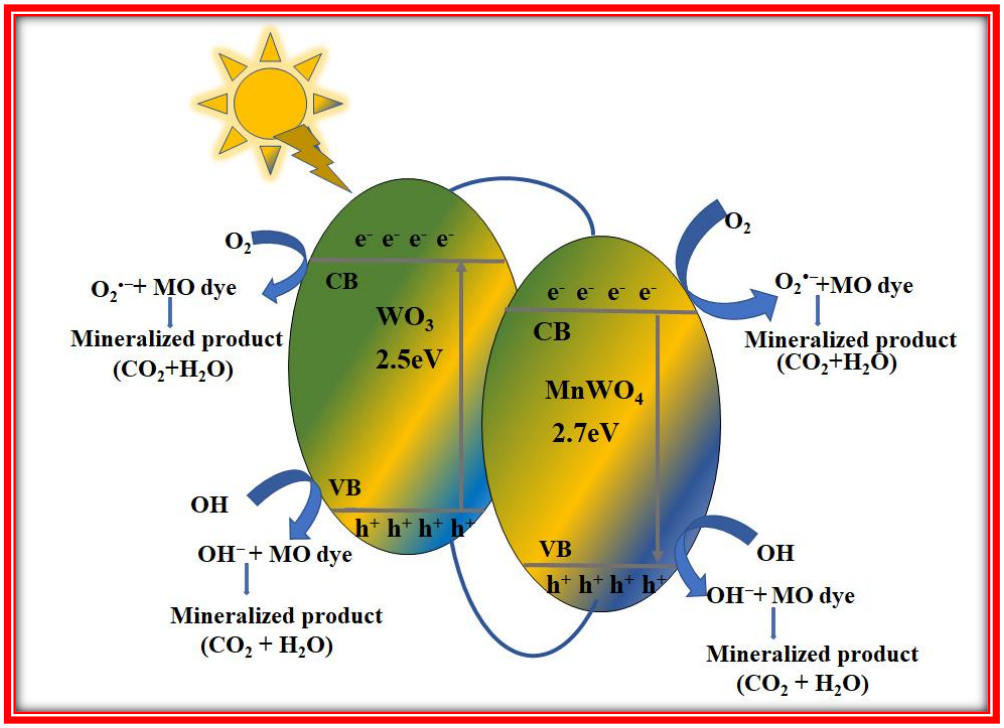

Figure 18. Graphical abstract of the photocatalytic degradation process of MO dye by the WO_3 and $MnWO_4$ nanocomposites.

4. Conclusions

This experiment of hydrothermal synthesis and characterization of WO_3 and $MnWO_4$ nanomaterials and evaluation of their photocatalytic activity proves that hydrothermal synthesis is an efficient and economical way for synthesizing the nanocomposites and WO_3 and MnWO4 nanomaterials are efficient photocatalysts. The physicochemical properties of the prepared nanomaterials were proven by thorough characterization using various analytical techniques like TEM, SEM, XRD, FT-IR, XPS. Similarly, the evaluation of the photocatalytic activity demonstrated the efficiency of WO_3 and $MnWO_4$ by their degradation ability against the potent organic pollutant MO dye. According to the results, in the optimal environment, WO_3 showed 50% degradation, whereas the $MnWO_4$ delivered 61% degradation against MO dye within the defined time of the experiment. This experiment and the photocatalytic activity proved that the homogenous nanomaterial, such as WO_3, when heterogeneously fabricated with metal oxide like Mn, can exhibit enhanced degradation efficiency than being deployed as a homogenous nanocomposite. Due to their outstanding and stable photocatalytic properties, the $MnWO_4$ nanocomposites can be used in various highly competent photocatalytic processes and various sensors, self-cleaning applications, and electrocatalytic applications.

Funding

This research received no external funding.

Acknowledgments

This research has no acknowledgment.

Conflicts of Interest

The authors declare no conflict of interest.

References

1. Thirumalai, K.; Shanthi, M.; Swaminathan, M. Ho2WO6/ZnO nanoflakes for photo–electrochemical and self cleaning applications. *Materials Science in Semiconductor Processing* **2019**, *90*, 78-86, https://doi.org/10.1016/j.mssp.2018.10.007.
2. Kumar, E.T.D.; Thirumalai, K.; Aravindhan, R.; Swaminathan, M.; Rao, J.R.; Nair, B.U. Visible light photocatalytic degradation of wattle extract: effect of mixing CdWO4 over a semiconductive ZnO photocatalyst. *RSC Advances* **2015**, *5*, 60926-60937, https://doi.org/10.1039/C5RA06926B.
3. Thirumalai, K.; Shanthi, M.; Swaminathan, M. Highly active Rare Earth (RE) Vanadate, Tungstate loaded ZnO (RE= Gd, Dy and Ho) Nanocomposites for Electrochemical methanol Oxidation-A Comparative study for Fuel cell Application. *Materials Today: Proceedings* **2018**, *5*, 15342-15347, https://doi.org/10.1016/j.matpr.2018.05.015.
4. Rajesh, G.; Akilandeswari, S.; Govindarajan, D.; Thirumalai, K. Enhancement of photocatalytic activity of ZrO2 nanoparticles by doping with Mg for UV light photocatalytic degradation of methyl violet and methyl blue dyes. *Journal of Materials Science: Materials in Electronics* **2020**, *31*, 4058-4072, https://doi.org/10.1007/s10854-020-02953-3.
5. Saravanakumar, K.; Mamba, G.; Muthuraj, V. 1D/2D MnWO4 nanorods anchored on g-C3N4 nanosheets for enhanced photocatalytic degradation ofloxacin under visible light irradiation. *Colloids Surf. A: Physicochem.Eng. Asp.***2019**, *581*, https://doi.org/10.1016/j.colsurfa.2019.123845.
6. Aliasghari, H.; Arabi, A.M.; Haratizadeh, H. A novel approach for solution combustion synthesis of tungsten oxide nanoparticles for photocatalytic and electrochromic applications. *Ceramics International* **2020**, *46*, 403-414, https://doi.org/10.1016/j.ceramint.2019.08.275.
7. Hatel, R.; Goumri, M.; Ratier, B.; Baitoul, M. Graphene derivatives/Fe3O4/polymer nanocomposite films: Optical and electrical properties. *Materials Chemistry and Physics* **2017**, *193*, 156-163, https://doi.org/10.1016/j.matchemphys.2017.02.013.
8. Wu, D.; Su, X.; Guo, W. Enhanced Photocatalytic Degradation of Methylene Blue over Hexagonal WO3/Graphene under Visible-Light Irradiation. *Kinetics and Catalysis* **2017**, *58*, 710-719, https://doi.org/10.1134/S0023158418010159.
9. Cui, H.; Shao, M.; Li, B.; Zhang, Y.; Yao, C.; Li, Z.; Xu, S. Facile fabrication of MnWO4/CdS composites for visible-light-driven photocatalytic Cr(VI) reduction. *Journal of Physics and Chemistry of Solids* **2020**, *136*, https://doi.org/10.1016/j.jpcs.2019.109150.
10. Yan, X.; Liu, K.; Shi, W. Facile synthesis of CdS/MnWO4 heterojunction with enhanced visible-light-driven photocatalytic activity and mechanism investigation. *Colloids and Surfaces A: Physicochemical and Engineering Aspects* **2017**, *520*, 138-145, https://doi.org/10.1016/j.colsurfa.2017.01.065.
11. Nawaz, A.; Rani, A.; Zarrin, H.; Saravanan, P. Construction of highly efficient separable p-n junction based light driven composite (NiFe2O4/MnWO4) for improved solar light utilisation. *Colloids and Surfaces A: Physicochemical and Engineering Aspects* **2022**, *642*, https://doi.org/10.1016/j.colsurfa.2022.128716.
12. Mao, J.; Zhao, J.; Li, L.; Chen, T.; Lv, Q.; Li, Y. Effect of different surfactants on the morphology, growth and magnetic behavior of MnWO4 crystals via the hydrothermal method. *Chinese Journal of Physics* **2020**, *63*, 163-167, https://doi.org/10.1016/j.cjph.2019.11.002.
13. Lima, A.E.B.; Assis, M.; Resende, A.L.S.; Santos, H.L.S.; Mascaro, L.H.; Longo, E.; Santos, R.S.; Cavalcante, L.S.; Luz, G.E. CuWO4|MnWO4 heterojunction thin film with improved photoelectrochemical and photocatalytic properties using simulated solar irradiation. *Journal of Solid State Electrochemistry* **2022**, *26*, 997-1011, https://doi.org/10.1007/s10008-022-05143-9.
14. Wu, J.; Xie, R.; Hu, X.; Nie, Z.; Shi, Y.; Yu, Y.; Yang, N. High-performance overall water splitting based on amorphous iron doped cobalt tungstate via facile co-precipitation. *Journal of Materials Chemistry A* **2021**, *9*, 9753-9760, https://doi.org/10.1039/D1TA00001B.
15. Thilagavathi, T.; Venugopal, D.; Thangaraju, D.; Marnadu, R.; Palanivel, B.; Imran, M.; Shkir, M.; Ubaidullah, M.; AlFaify, S. A facile co-precipitation synthesis of novel WO3/NiWO4 nanocomposite with improved photocatalytic activity. *Materials Science in Semiconductor Processing* **2021**, *133*, https://doi.org/10.1016/j.mssp.2021.105970.
16. Sundaresan, R.; Mariyappan, V.; Chen, S.-M.; Keerthi, M.; Ramachandran, R. Electrochemical sensor for detection of tryptophan in the milk sample based on MnWO4 nanoplates encapsulated RGO nanocomposite. *Colloids and Surfaces A: Physicochemical and Engineering Aspects* **2021**, *625*, https://doi.org/10.1016/j.colsurfa.2021.126889.
17. Mahieddine, A.; Adnane-Amara, L.; Gabouze, N.; Addad, A.; Swaidan, A.; Boukherroub, R. Self-combustion synthesis of dilithium cobalt bis(tungstate) decorated with silver nanoparticles for high performance hybrid supercapacitors. *Chemical Engineering Journal* **2021**, *426*, https://doi.org/10.1016/j.cej.2021.131252.
18. Nandiyanto, A.B.D.; Zaen, R.; Oktiani, R. Working Volume in High-Energy Ball-Milling Process on Breakage Characteristics and Adsorption Performance of Rice Straw Ash. *Arabian Journal for Science and Engineering* **2018**, *43*, 6057-6066, https://doi.org/10.1007/s13369-018-3265-4.

19. Khanam, S.; Rout, S.K. Decolourization of rhodamine B and methylene blue dyes in the presence of bismuth tungstates: a detailed investigation on the effect of grain size. *Bulletin of Materials Science* **2021**, *44*, 1-7, https://doi.org/10.1007/s12034-020-02292-3.
20. Mohammadikish, M.; Masteri-Farahani, M.; Mahdian, T. Optical properties of copper tungstate nanoparticles prepared by microemulsion method. *Inorganic and Nano-Metal Chemistry* **2019**, *49*, 63-68, https://doi.org/10.1080/24701556.2019.1600550.
21. Zinatloo-Ajabshir, S.; Baladi, M.; Salavati-Niasari, M. Sono-synthesis of MnWO4 ceramic nanomaterials as highly efficient photocatalysts for the decomposition of toxic pollutants. *Ceramics International* **2021**, *47*, 30178-30187, https://doi.org/10.1016/j.ceramint.2021.07.197.
22. Yusuf, M.; Hira, S.A.; Park, K.H. Light-Harvesting Novel Hierarchical Porous Cu9S5–MnWO4 Hybrid Structures in Photocatalytic Oxidative Homocoupling of Alkynes and Amines. *ACS Applied Materials & Interfaces* **2022**, *14*, 15529-15540, https://doi.org/10.1021/acsami.2c00279.
23. Khoobi, A.; Shahdost-fard, F.; Arbabi, M.; Akbari, M.; Mirzaei, H.; Nejati, M.; Lotfinia, M.; Sobhani-Nasab, A.; Banafshe, H.R. Sonochemical synthesis of ErVO4/MnWO4 heterostructures: Application as a novel nanostructured surface for electrochemical determination of tyrosine in biological samples. *Polyhedron* **2020**, *177*, https://doi.org/10.1016/j.poly.2019.114302.
24. Kumar, K.S.; Vaishnavi, K.; Venkataswamy, P.; Ravi, G.; Ramaswamy, K.; Vithal, M. Photocatalytic degradation of methylene blue over N-doped MnWO4 under visible light irradiation. *Journal of the Indian Chemical Society* **2021**, *98*, https://doi.org/10.1016/j.jics.2021.100140.
25. Li, Y.; Wu, X.; Chen, J.; Cao, A.; Boudaghi, R.; Akhtar, M.N. Effect of filler loading and thickness parameters on the microwave absorption characteristic of double-layered absorber based on MWCNT/BaTiO3/pitted carbonyl iron composite. *Ceramics International* **2021**, *47*, 19538-19545, https://doi.org/10.1016/j.ceram.int.2021.03.291.
26. Uribe-López, M.C.; Hidalgo-López, M.C.; López-González, R.; Frías-Márquez, D.M.; Núñez-Nogueira, G.; Hernández-Castillo, D.; Alvarez-Lemus, M.A. Photocatalytic activity of ZnO nanoparticles and the role of the synthesis method on their physical and chemical properties. *Journal of Photochemistry and Photobiology A: Chemistry* **2021**, *404*, https://doi.org/10.1016/j.jphotochem.2020.112866.
27. Wang, X.; Sø, L.; Su, R.; Wendt, S.; Hald, P.; Mamakhel, A.; Yang, C.; Huang, Y.; Iversen, B.B.; Besenbacher, F. The influence of crystallite size and crystallinity of anatase nanoparticles on the photodegradation of phenol. *Journal of Catalysis* **2014**, *310*, 100-108, https://doi.org/10.1016/j.jcat.2013.04.022.
28. Vilian, A.T.E.; Oh, S.Y.; Rethinasabapathy, M.; Umapathi, R.; Hwang, S.-K.; Oh, C.W.; Park, B.; Huh, Y.S.; Han, Y.-K. Improved conductivity of flower-like MnWO4 on defect engineered graphitic carbon nitride as an efficient electrocatalyst for ultrasensitive sensing of chloramphenicol. *Journal of Hazardous Materials* **2020**, *399*, https://doi.org/10.1016/j.jhazmat.2020.122868.
29. Jiang, Y.N.; Liu, B.D.; Yang, W.J.; Yang, B.; Liu, X.Y.; Zhang, X.L.; Mohsin, M.A.; Jiang, X. New strategy for the in situ synthesis of single-crystalline MnWO4/TiO2 photocatalysts for efficient and cyclic photodegradation of organic pollutants. *CrystEngComm* **2016**, *18*, 1832-1841, https://doi.org/10.1039/C5CE02445E.
30. Sethi, Y.A.; Kulkarni, A.K.; Ambalkar, A.A.; Khore, S.K.; Gunjal, A.R.; Gosavi, S.W.; Kale, B.B. CdS decorated MnWO4 nanorod nanoheterostructures: a new 0D–1D hybrid system for enhanced photocatalytic hydrogen production under natural sunlight. *Nanoscale Advances* **2021**, *3*, 508-516, https://doi.org/10.1039/D0NA00843E.
31. Askari, N.; Beheshti, M.; Mowla, D.; Farhadian, M. Facile construction of novel Z-scheme MnWO4/Bi2S3 heterojunction with enhanced photocatalytic degradation of antibiotics. *Materials Science in Semiconductor Processing* **2021**, *127*, https://doi.org/10.1016/j.mssp.2021.105723.
32. Sardar, K.; Thakur, S.; Maiti, S.; Besra, N.; Bairi, P.; Chanda, K.; Majumdar, G.; Chattopadhyay, K.K. Amalgamation of MnWO4 nanorods with amorphous carbon nanotubes for highly stabilized energy efficient supercapacitor electrodes. *Dalton Transactions* **2021**, *50*, 5327-5341, https://doi.org/10.1039/D1DT00267H.
33. Balasurya, S.; Okla, M.K.; Alaraidh, I.A.; Soufan, W.; Al-ghamdi, A.A.; Ahamad, S.R.; Abdel-Maksoud, M.A.; AbdElgawad, H.; Raju, L.L.; Thomas, A.M.; Khan, S.S. Photodegradation of 5-flurouracil, carvedilol, para-chlorophenol and methimazole with 3D MnWO4 nanoflower modified Ag2WO4 nanorods: A non-genotoxic nanomaterial for water treatment. *Chemosphere* **2022**, *297*, https://doi.org/10.1016/j.chemosphere.2022.134130.
34. Muthamizh, S.; Suresh, R.; Giribabu, K.; Manigandan, R.; Praveen Kumar, S.; Munusamy, S.; Narayanan, V. MnWO4 nanocapsules: Synthesis, characterization and its electrochemical sensing property. *Journal of Alloys and Compounds* **2015**, *619*, 601-609, https://doi.org/10.1016/j.jallcom.2014.09.049.
35. Peixoto, J.C.; Nogueira, A.E.; Dias, A.; Torres, J.A.; da Cruz, J.C.; Ribeiro, C.; Siqueira, K.P.F. Experimental evaluation of the activity and selectivity of pure MnWO4 and doped with rare earth ions in the CO2 photoreduction process. *Materials Research Bulletin* **2022**, *153*, https://doi.org/10.1016/j.materresbull.2022.111912.
36. Meziani, D.; Roumila, Y.; Ghoul, N.Y.; Benmeriem, D.; Abdmeziem, K.; Trari, M. Physicochemical characterizations and semiconducting properties of a manganese tungstate MnWO4 obtained by

hydrothermal route. *Journal of Solid State Electrochemistry* **2021**, *25*, 2097-2106, https://doi.org/10.1007/s10008-021-04977-z.
37. Joaquín-Morales, M.G.; Fuentes, A.F.; Montemayor, S.M.; Meléndez-Zaragoza, M.J.; Gutiérrez, J.M.S.; Ortiz, A.L.; Collins-Martínez, V. Synthesis conditions effect on the of photocatalytic properties of MnWO4 for hydrogen production by water splitting. *International Journal of Hydrogen Energy* **2019**, *44*, 12390-12398, https://doi.org/10.1016/j.ijhydene.2018.10.075.
38. Widiyandari, H.; Firdaus, I.; Kadarisman, V.G.S.; Purwanto, A. Optical properties and photocatalytic activities of tungsten oxide (WO3) with platinum co-catalyst addition. *AIP Conference Proceedings* **2016**, *1712*, https://doi.org/10.1063/1.4941910.
39. Vengatachalam, M.; Ramakrishnan, E.; Revathi, P.; Umapathy, V.; Suganya, P.; Krishnasamy, K. Synthesis, Characterization, Photocatalytic and Electrochemical Studies of Reduced Graphene Oxide Doped Nickel Oxide Nanocomposites. *Asian Journal of Chemistry* **2021**, *33*, 411-422, https://doi.org/10.14233/ajchem.2021.22979.
40. Askari, N.; Beheshti, M.; Mowla, D.; Farhadian, M. Facile construction of novel Z-scheme MnWO4/Bi2S3 heterojunction with enhanced photocatalytic degradation of antibiotics. *Materials Science in Semiconductor Processing* **2021**, *127*, https://doi.org/10.1016/j.mssp.2021.105723.
41. Le, A.T.; Samsuddin, N.S.B.; Chiam, S.-L.; Pung, S.-Y. Synergistic effect of pH solution and photocorrosion of ZnO particles on the photocatalytic degradation of Rhodamine B. *Bulletin of Materials Science* **2021**, *44*, 1-10, https://doi.org/10.1007/s12034-020-02281-6.
42. Kumar, O.P.; Ahmad, M.; Nazir, M.A.; Anum, A.; Jamshaid, M.; Shah, S.S.A.; Rehman, A. Strategic combination of metal–organic frameworks and C3N4 for expeditious photocatalytic degradation of dye pollutants. *Environmental Science and Pollution Research* **2022**, *29*, 35300-35313, https://doi.org/10.1007/s11356-021-17366-w.
43. Ramar, V.; Balasubramanian, K. Reduced Graphene Oxide/WO3 Nanorod Composites for Photocatalytic Degradation of Methylene Blue under Sunlight Irradiation. *ACS Applied Nano Materials* **2021**, *4*, 5512-5521, https://doi.org/10.1021/acsanm.1c00863.
44. Guo, J.; Sun, H.; Yuan, X.; Jiang, L.; Wu, Z.; Yu, H.; Tang, N.; Yu, M.; Yan, M.; Liang, J. Photocatalytic degradation of persistent organic pollutants by Co-Cl bond reinforced CoAl-LDH/Bi12O17Cl2 photocatalyst: mechanism and application prospect evaluation. *Water Research* **2022**, *219*, https://doi.org/10.1016/j.watres.2022.118558.